IEEE Access
Multidisciplinary ⋮ Rapid Review ⋮ Open Access Journal

Received March 21, 2020, accepted April 10, 2020, date of publication April 14, 2020, date of current version April 29, 2020.

Digital Object Identifier 10.1109/ACCESS.2020.2987908

Feedback Linearization Kalman Observer Based Sliding Mode Control for Semi-Active Suspension Systems

ZHENG LIU, HONGBIN REN, (Member, IEEE), SIZHONG CHEN, YONG CHEN, AND JIANBO FENG

School of Mechanical Engineering, Beijing Institute of Technology, Beijing 100081, China

Corresponding author: Hongbin Ren (renhongbin2106@126.com)

This work was supported by the National Natural Science Foundation of China under Grant 51375046 and Grant 51205021.

ABSTRACT In this paper, a new approach for an observer based controller for semi-active suspension systems is presented. The observer part is a feedback linearization Kalman filter which is based on differential geometry. The original nonlinear system is transferred to a linear system by certain coordinate transfer after the verification of observability and solvability of the system observer design problem under certain sensor placement configurations. Then, a linear Kalman filter algorithm can be applied to the linearized system. The state information can be obtained through an inverse coordinate transfer of the estimation results of the linear Kalman filter. The observer is verified by a simulation test under different road profiles, and a comparison between the designed observer and extended Kalman filter shows that the feedback linearization Kalman filter has better performance. A model reference sliding mode controller based on the estimation results of the observer is also proposed. A rig test system for the semi-active suspension system is implemented, and, both the designed observer and controller are verified through the rig test. Experimental results show that the proposed new approach for semi-active suspension control can significantly improve vehicle ride comfort with common and low-cost sensors.

INDEX TERMS Semi-active suspension, feedback linearization, Kalman filter, observer design.

I. INTRODUCTION

A suspension system for a vehicle can suspend the spring mass while maintaining contact between the wheel and the road surface. Performance of the suspension is often assessed in terms of ''ride comfort'' and ''ride handling''. Active suspension systems have been proven to be able to manage these conflicting trade-offs better than with traditional passive suspension. However, active suspension systems are complex, expensive, and high-energy consuming, and thus, barely implemented on mass-production vehicles. Semi-active suspension overcomes the abovementioned disadvantages of active suspension with only a small reduction in performance. Another advantage of the semi-active suspension over active suspension is that the semi-active suspension has a ''fail-safe'' feature, which turns the semi-active suspension into a passive suspension when the control system malfunctions. As the semi-active suspension has been widely commercialized, the control strategy, as the key factor that influences the performance of the semi-active suspension system, has attracted increasing attention from researchers.

Control algorithms introduced by early researchers such as optimal control [1]–[3] and skyhook control [4]–[6] are mainly linear controllers. These control strategies cannot reflect the nonlinear characteristic of the vehicle [7]; however, those control strategies are not robust enough under parameter variations and perturbations. To solve these problems, new techniques, such as sliding mode control [8]–[18], fuzzy logic [14], [19]–[21], and neural networks [22]–[24], have been introduced to the design process of semi-active suspension controllers. However, the stability of intelligence controllers is hard to prove mathematically, which limits its application for vehicle suspension systems. Sliding mode control is a kind of variable structure control that changes the structure of the system with a discontinuous signal. It has proven effective and robust under system perturbation and external disturbances for both linear and nonlinear systems. Since actual suspension systems contain different kinds of

The associate editor coordinating the review of this manuscript and approving it for publication was Mouloud Denai.

This work is licensed under a Creative Commons Attribution 4.0 License. For more information, see https://creativecommons.org/licenses/by/4.0/

uncertainties and require high control robustness, a sliding mode controller is suitable for practical applications. Xinbo proposed a particle swarm optimization based sliding mode control for precise desired damping force control. The proposed controller was verified through hardware in the loop test [9]. Nguyen proposed a fuzzy disturbance observer enhanced sliding mode observer for a semi-active suspension equipped with a magneto-rheological damper. Comparative work with other existing controllers shows that the proposed method can provide better vibration control and consume relatively low energy at the same time [25]. Ren combined UKF and a sliding mode controller for an approach of semi-active suspension control systems. A hybrid reference model was presented for the sliding mode controller for a better compromise between ride comfort and ride handling. Both the observer and the controller were verified by simulation tests [16].

Most control strategies rely on the assumption that all the states, or at least the states they need, can be measured accurately. However, this assumption is usually too demanding and sometimes even technically unfeasible. In particular, the absolute vertical velocity of the spring mass cannot be measured directly with sensors. The common technique widely used in engineering applications to integrate acceleration signals for speed suffers considerably from DC offset. At present, the most appropriate solution for the abovementioned problem is to design a state observer to estimate state information from easily accessible measurements. The Kalman filter is a widely used observer algorithm, whose effectiveness has been proven for the semi-active suspension systems. However, also known as linear quadratic estimation, the Kalman filter is a linear algorithm that can not be directly applied to nonlinear systems. Therefore, nonlinear versions of the Kalman filter have been introduced by researchers [26]–[29]. Reina implemented an extended Kalman filter (EKF) for lateral dynamics of a half vehicle model for tyre cornering stiffness identification [30]. Wei combined the minimum model error with EKF to design a state observer for 4WD vehicle states [31]. Simulation results show that the designed observer has better accuracy compared with traditional EKF. The principle of the EKF is to linearize the nonlinear system by Taylor expansion and first-order approximation. However, this linearization method may lead to deterioration of estimation results when the system is far from the equilibrium point [32]. Another nonlinear version of the Kalman filter is the unscented Kalman filter (UKF). The UKF solves the problem of obtaining the state mean and covariance matrix by means of unscented transformation and sigma points propagation and is believed to have better accuracy than the EKF in most nonlinear model cases. Ren designed a UKF observer-based hybrid sliding mode controller for suspension systems, and the accuracy of the observer was verified through simulation road tests [16]. López combined the UKF and adaptive network-based fuzzy inference system (ANFIS) to estimate vehicle sideslip angle, the designed estimator was verified under different driving maneuvers [33]. Apart from the KF and its nonlinear versions, other methods have also been implemented in the field of vehicle state estimation. Olma designed a sliding mode observer for the parallel kinematic excitation unit [34]. The designed observer was implemented in a real-time environment and was verified through hardware in loop simulation tests. A robust observer was designed by Alfonso in the H-infinity framework for the damping force of a semi-active suspension system equipped with an electro-rheological damper [35]. A Luenberger observer was designed by Giua. The working principle of the designed observer is to minimize the H_2 norm of the transfer function matrix among the error state estimations [36]. A simulation was performed to verify the observer considering both the solenoid valve damper and the magneto-rheological damper. Neural-network-technique-based observers do not rely on specific system models [37]–[40]. However, the accuracy of neural network observers depends on large quantities of training data, which sometimes is not easy to acquire.

The nonlinear character of the system has always been a difficult point of observer design. The general method for solving a nonlinear system observer design problem is to linearize the nonlinear system and apply a linear algorithm to the linearized system. Traditional linearization techniques such as the EKF are based on series expansion and first-order approximation. The neglected high-order parts of the original nonlinear system cause nonnegligible errors when the system state is far from the equilibrium point.

The aim of this paper is to provide a new approach for an observer-based controller for a semi-active suspension system with nonlinear damping force character. Though widely used and proven effective in the field of controller design, the feedback linearization technique has rarely been used as a linearization technique for state observers especially for multi-output systems such as the semi-active suspension system presented in the paper. In this paper, a feedback linearization based Kalman observer is proposed. Its main principle is to find a specific coordinate transfer which can turn the original nonlinear system into a linear system. Then, a linear Kalman filter algorithm can be applied to the linearized system. The state information of the original system can be obtained through reverse coordinate transfer. Furthermore, to verify the designed observer's ability to provide accurate enough state estimations for the controller, a model reference sliding mode controller is designed. The effectiveness of both the observer and the observer-based controller is verified through rig tests.

This paper is organized as follows. A nonlinear quarter car dynamic model equipped with a solenoid valve-based adjustable damper is presented in section 2. Feedback linearization and the observer design process of the quarter car system presented in the previous section are explained in detail in section 3. Section 4 shows the simulation results of the designed observer and its comparison with the EKF. Accuracy analysis of the observer under a disturbance is also performed in section 4. In section 5, a model reference

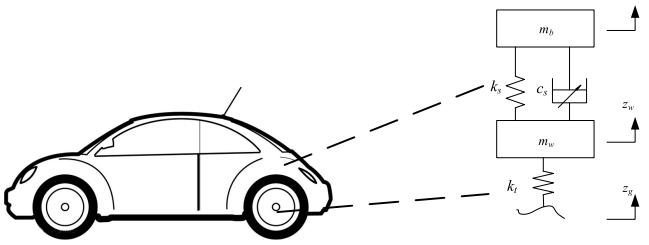

FIGURE 1. Nonlinear quarter car model.

sliding mode controller based on the state information of the previously designed observer is implemented. A rig test system is implemented, and an experiment is performed to verify the observer based controller in the last section.

II. SYSTEM MODELING

The linear model can only reflect the vehicle's dynamic characteristics when the system is around the equilibrium position. Out of this range, the deviation caused by the linear model cannot be ignored. Therefore, it is essential to build a nonlinear model for the research of nonlinear suspension systems. In our case, the variable force element of a semi-active suspension is an adjustable damper equipped with a solenoid valve.

A quarter car model is a two DOF (degrees of freedom) model, which can reflect the vertical motion of the vehicle. It is often used for suspension observer/controller design purposes.

As the figure above shows, the nonlinear quarter car model has two degrees: the vertical displacement of sprung and unsprung mass. In the figure, m_b is the sprung mass, z_b is the sprung mass vertical displacement, m_w is the unsprung mass, z_w is the unsprung mass vertical displacement, and z_g is the road profile. The stiffness coefficient is k_s for semi-active suspension systems, and the damping coefficient c_s is not a constant value. k_t is the stiffness coefficient of the tyre and the damping force of the tyre is assumed to be negligible.

State equations for the model are:

$$\begin{aligned} m_b\ddot{z}_b &= -F_s(z_b - z_w) - F_d(\dot{z}_b - \dot{z}_w), \\ m_w\ddot{z}_w &= F_s(z_b - z_w) + F_d(\dot{z}_b - \dot{z}_w) - k_t \cdot (z_w - z_g). \end{aligned} \quad (1)$$

where F_s is the spring force function and F_d is the damping force function.

The research object of this paper is a solenoid valve-based adjustable damper. The main feature of the solenoid damper is the electro valve which can regulate the damping coefficient according to the control current. The voltage of the control current is proportional to the duty ratio of the PWM signal. According to the working principle of the solenoid valve-based adjustable damper, its damping force is the function of control current and suspension deflection velocity. The precise damping force characteristic of the adjustable damper used in this paper was obtained through a rig test.

Asymptotic displacement is given to the damper by the excitation joint of the test rig under a given control current.

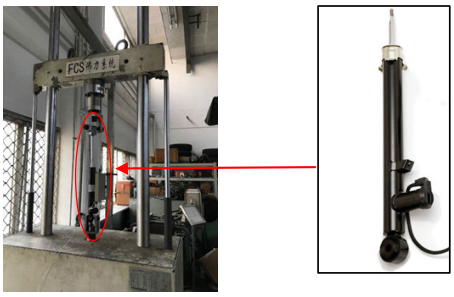

FIGURE 2. Damping force characteristic rig test.

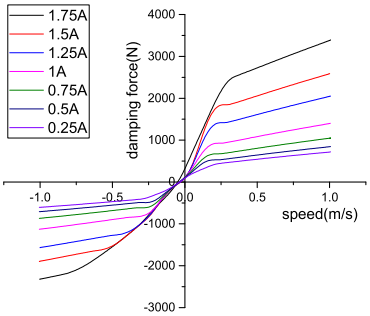

FIGURE 3. Damping force characteristic of the damper under different control currents.

The displacement and damping force signal is then recorded by the host pc. The test procedure is repeated under different control currents of the damper. Then, the damping force characteristic of the adjustable damper under different control currents can be drawn.

Figure 3 shows the changing pattern of the damping force under different control currents. Generally, the damping force under the same suspension speed increases when the larger control current is given the damper. However, medium damping force is outputted by the damper when its control current is set to zero. The reason for this phenomenon is that the solenoid valve-based semi-active suspension has a so-called "fail-safe" mode, which can make the damper behave as a passive suspension damper even if the control system fails. When the control current is set to 0.25A, the damper has the smallest damping force. When controlling the adjustable damper, only the control current section from 0.25A to 1.75A is used.

III. FEEDBACK LINEARIZATION KALMAN OBSERVER DESIGN

The feedback linearization technique in observer design is based on differential geometry theory. In addition, its main principle is to establish a proper coordinate transformation to the nonlinear system so that precise feedback linearization of the original system can be achieved. For the following nonlinear system

$$\begin{cases} \dot{x} = f(x), \\ y = h(x). \end{cases} \quad (2)$$

TABLE 1. Feasible sensor placement configurations for quarter vehicle systems.

Measurement variables	Sensor placement configurations									
	①	②	③	④	⑤	⑥	⑦	⑧	⑨	⑩
$\ddot{z}_b$	●				●		●		●	
$\dot{z}_b$		●			●			●		●
$(z_b - z_w)$			●			●	●	●		
$(\dot{z}_b - \dot{z}_w)$				●		●			●	●

where x is the system state space vector, y is the system output vector, f is the system state space function, h is the system output function b is the function of y.

When certain proper coordinate transfer x = X(ξ) is adopted by the nonlinear system, the original nonlinear system can be transformed into the following form:

$$\begin{cases} \dot{\xi} = A\xi + b(y), \\ y = h(X(\xi)) = C\xi. \end{cases} \tag{3}$$

Here, ξ is the state vector of the transformed linear system.

Before the system feedback linearization process, it is important to define the system state space and verify the system observability and solvability of the observer design problem.

The main motivation of the state observer design in our paper is to obtain state information that cannot be measured or is too difficult to be directly measured by sensors such as spring-mass vertical speed from signals, which can be directly measured from commonly used and low-cost sensors.

For our quarter car nonlinear system, there are at least 10 possible sensor configurations, which are listed below.

In the above table, both acceleration sensors and relative displacement sensors are common and low cost.

The state vector is defined as $x = [\dot{z}_b,\ \dot{z}_w,\ z_b - z_w, z_w - z_g]^T$. The process noise and measurement noise is considered, so the nonlinear system can be expressed as:

$$\begin{cases} \dot{x} = f(x) + G \cdot w \\ y_m = h_y(x) + v \end{cases} \tag{4}$$

where $w = \dot{z}_g$ is the process noise; v is the measurement noise.

$$f(x) = \begin{bmatrix} -\dfrac{F_d(x_1 - x_2)}{m_b} - \dfrac{F_s(x_3)}{m_b} \\ \dfrac{F_d(x_1 - x_2)}{m_w} + \dfrac{F_s(x_3)}{m_w} - \dfrac{k_t}{m_w}x_4 \\ x_1 - x_2 \\ x_2 \end{bmatrix}. \tag{5}$$

$$G = [0, 0, 0, -1]^T. \tag{6}$$

The form of y_m and $h_y(x)$ depends on the selection of sensor displacement configuration. In addition, before attempting to obtain the proper coordinate to accomplish the linearize process, it is important to verify the system observability and solvability under different sensor placement configurations.

For a better explanation of the observability and solvability verification of the system, the following deduction is under sensor placement configuration ⑥, which is also our final selection for observer design. Under sensor placement configuration ⑥, the corresponding form of y_m and $h_y(x)$ is:

$$y = [y_1, y_2]^T = [\,\dot{z}_b - \dot{z}_w,\ z_b - z_w\,]^T. \tag{7}$$

$$h_y(x) = [h_1(x), h_2(x)] = [x_1 - x_2, x_3]. \tag{8}$$

A. SYSTEM OBSERVALITY VERIFICATION

Here, we have the dimension of the system n=4 and the dimension of the output function m=2. A K dimension real sequence $L = \{l_0, \cdots, l_{k-1}\}$ is defined which meets:

$$m = l_0 \geq \cdots \geq l_{k-1} > 0, \quad \sum_{i=0}^{k-1} l_i = n. \tag{9}$$

According to differential geometry theory [41], the system is observable *iff* (if and only if) observer matrix Q is nonsingular; the form of Q is

$$Q = \begin{bmatrix} dh_{(1)} \\ L_f(dh_{(2)}) \\ \vdots \\ L_f^{k-1}(dh_{(k)}) \end{bmatrix}, \quad h_{(i)} = \left[\, h_1,\ h_2,\ \cdots,\ h_{l_{i-1}} \,\right]^T. \tag{10}$$

Elements of matrix Q are the partial derivative and Lie derivative of elements of the output function.

When the elements of matrix Q are calculated, we can obtain

$$dh_1 = \left[\, 1,\ -1,\ 0,\ 0 \,\right]. \tag{11}$$

where $d\alpha$ is the condensed notation of $\partial\alpha/\partial x$.

$$L_f(dh_1) = \left[-\frac{dF_d}{m_e}, \frac{dF_d}{m_e}, -\frac{dF_s}{m_e}, \frac{k_t}{m_w} \right]. \tag{12}$$

$$L_f^2(dh_1) = \left[A_1, -A_1 + \frac{k_t}{m_w}, A_2, -\frac{k_t}{m_w}\frac{dF_d}{m_e} \right]. \tag{13}$$

$$L_f^3(dh_1) = \left[A_3 + \frac{k_t}{m_w}\frac{dF_d}{m_w}, -A_3 - \frac{k_t}{m_w}\left(\frac{dF_d}{m_w} + \frac{dF_d}{m_e}\right), A_4, A_5 \right]. \tag{14}$$

$$dh_2(x) = \left[\, 0, \quad 0, \quad 1, \quad 0 \,\right]. \tag{15}$$

$$L_f^i(dh_2) = L_f^{i+1}(dh_1), \quad i = 1, 2, 3. \tag{16}$$

Limited by the length of the paper, expressions of A_i and m_e are listed in the appendix of this paper.

Substitute (11) to (16) into (9), and it can be verified that when the real sequence defined in (9)

$$L = \left\{\, l_0,\ l_1,\ l_2 \,\right\} = \left\{\, 2,\ 1,\ 1 \,\right\}. \tag{17}$$

matrix Q is full rank, and the system is observable.

B. SYSTEM COORDINATE TRANSFER SOLVING

Define,

$$h_{I,0} = \begin{bmatrix} h_1 \\ h_2 \end{bmatrix}, \quad h_{II,0} = \emptyset,\ h_{I,1} = h_1,$$

$$h_{II,1} = h_2, \quad h_{I,2} = h_1, \ h_{II,2} = h_2. \tag{18}$$

$$Q_j = \begin{bmatrix} dh \\ \vdots \\ L_f^{j-1}(dh) \end{bmatrix},$$

$$Q_{I,j} = \begin{bmatrix} dh_{I,0} \\ \vdots \\ L_f^{j-1}(dh_{I,j-1}) \end{bmatrix}, \quad j = 1, \cdots, k,$$

$$Q_{I,1} = dh_{I,0}, \quad Q_{I,2} = \begin{bmatrix} dh_{I,0} \\ L_f(dh_{I,1}) \end{bmatrix},$$

$$Q_{I,3} = \begin{bmatrix} dh_{I,0} \\ L_f(dh_{I,1}) \\ L_f^2(dh_{I,2}) \end{bmatrix}. \tag{19}$$

According to the conclusion of paper [41], the linearization problem of the system is solvable *iff* when

1)

$$L_f^j(dh_{II,j}) \in span Q_{I,j} + span_R\{L_f^j(dh_{I,j})\}, \quad j = 1, \cdots, k-1 \tag{20}$$

2) (A,C) which is also called the system observation matrix pair is in condensed Brunovský form:

$$\begin{cases} A = \begin{bmatrix} 0, & E_1, & & \\ & \ddots & \ddots & \\ & & \ddots & E_{k-1} \\ & & & 0 \end{bmatrix}, \quad C = \begin{bmatrix} C_1, & 0, & \cdots & 0 \end{bmatrix}, \\ E_i = [e_1, \cdots, e_{l_i}] \in R^{l_{i-1} \times l_i}. \end{cases} \tag{21}$$

where C_1 is a square and nonsingular matrix, and e_i is the ith column of the l_{i-1}-dimensional unit matrix.

Substitute (11) to (19) into (20) and it can be easily verified that (20) is met.

And when

$$A = \begin{bmatrix} 0, & 0, & 1, & 0 \\ 0, & 0, & 0, & 0 \\ 0, & 0, & 0, & 1 \\ 0, & 0, & 0, & 0 \end{bmatrix}, \quad C = \begin{bmatrix} 1, & 0, & 0, & 0 \\ 0, & 1, & 0, & 0 \end{bmatrix}. \tag{22}$$

For coordinate transfer $x = X(\xi)$ and derivative of the coordinate transfer $\partial X/\partial \xi = G$ where G has the form of

$$G = [\, g_1, \cdots, g_k \,]. \tag{23}$$

Again, from the proposition proven in [41], elements of matrix G should have the following form

$$\begin{aligned} Q_k g_k &= \tilde{E}_k, \quad Q_i g_i = \tilde{E}_i, \\ g_i E_i &= -ad_f g_{i+1}, \quad i = k-1, \cdots, 1. \end{aligned} \tag{24}$$

where,

$$\tilde{E}_i = \begin{bmatrix} 0, & \cdots, & \bar{E}_{i-1} \end{bmatrix}^T, \quad \bar{E}_i = \bar{E}_{i-1} E_i, \ \bar{E}_0 = I. \tag{25}$$

From the definition of the generalized inverse matrix, (25) equals

$$\begin{aligned} g_k = Q_k^- \tilde{E}_k, \, g_i = -ad_f g_{i+1} E_i^T + Q_i^- \tilde{E}_i (I - E_i E_i^T) \\ + (I - Q_i^- Q_i) Z_i (I - E_i E_i^T) \end{aligned} \tag{26}$$

where, $(\cdot)^-$ is an arbitrary inverse of $(\cdot)$ which satisfies $(\cdot)(\cdot)^{-1}(\cdot) = (\cdot)$, and Z_i is an arbitrary matrix of proper dimension.

Then, the derivative of the coordinate can be obtained

$$\frac{\partial X}{\partial \xi} = G = \begin{bmatrix} g_1, & g_2, & g_3 \end{bmatrix} = \begin{bmatrix} 0, & 0, & 0, & \frac{m_w}{k_t} \\ -1, & 0, & 0, & \frac{m_w}{k_t} \\ 0, & 1, & 0, & 0 \\ 0, & 0, & \frac{m_w}{k_t}, & 0 \end{bmatrix}. \tag{27}$$

Integrate (27) and, we can obtain coordinate transfer

$$x = X(\xi) = \begin{bmatrix} \frac{m_w}{k_t}\xi_4, & -\xi_1 + \frac{m_w}{k_t}\xi_4, & \xi_2, & \frac{m_w}{k_t}\xi_3 \end{bmatrix}^T. \tag{28}$$

And corresponding inverse coordinate transfer

$$\xi = T(x) = \begin{bmatrix} x_1 - x_2, & x_3, & \frac{k_t}{m_w}x_4, & \frac{k_t}{m_w}x_1 \end{bmatrix}^T. \tag{29}$$

C. SENSOR CONFIGURATION SELECTION

The verification and solving processes of sensor configuration ⑥ are repeated, and we can obtain the solution of the feedback linearization problem under each sensor placement configuration and the existing condition of the solutions.

1) Under sensor placement configuration ①, the solution existing condition for the solution is that the system has linear spring force and linear damping force. The solution is:

$$h = -\frac{F_d(x_1 - x_2)}{m_b} - \frac{F_s(x_3)}{m_b}, \quad y = y_1 = \ddot{z}_b. \tag{30}$$

$$\begin{aligned} X(\xi) = & \frac{1}{\frac{k_t}{m_w}\frac{dF_d}{m_b} + \frac{dF_s}{m_b}\frac{dF_s}{dF_d}} \\ & \times \begin{bmatrix} \left(-\frac{m_w}{k_t}\frac{dF_s}{dF_d} - \frac{dF_d}{dF_s}\right)\xi_4 \\ \frac{k_t}{m_w}\xi_1 + \frac{dF_s}{dF_d}\xi_2 - \xi_3 - \frac{m_w}{k_t}\frac{dF_s}{dF_d}\xi_4 \\ -\frac{dF_s}{dF_d}\xi_1 + \xi_2 - \frac{dF_d}{dF_s}\xi_3 + \frac{dF_d}{dF_s}\frac{dF_d}{dF_s}\xi_4 \\ \frac{dF_s}{dF_d}\xi_1 - \xi_2 - \frac{m_w}{k_t}\frac{dF_s}{dF_d}\xi_3 + \frac{m_w}{k_t}\xi_4 \end{bmatrix}. \end{aligned} \tag{31}$$

$$A = \begin{bmatrix} 0, & 1, & 0, & 0 \\ 0, & 0, & 1, & 0 \\ 0, & 0, & 0, & 1 \\ 0, & 0, & 0, & 0 \end{bmatrix}, \quad C = \begin{bmatrix} 1, & 0, & 0, & 0 \end{bmatrix}. \tag{32}$$

$$\begin{aligned} b(y) = & \left[-\frac{dF_d}{m_e}y_1, -\left(\frac{dF_s}{m_e} + \frac{k_t}{m_w}\right)y_1, \right. \\ & \left. -\frac{k_t}{m_w}\frac{dF_d}{m_b}y_1, -\frac{k_t}{m_w}\frac{dF_s}{m_b}y_1 \right]^T. \end{aligned} \tag{33}$$

2) Under sensor displacement configuration ②, the solution existing condition is linear spring and damping force. The solution is:

$$h = \dot{z}_b, \quad y = y_1 = \dot{z}_b. \tag{34}$$

$$x = X(\xi) = \frac{\begin{bmatrix} \left(\frac{k_t}{m_w}\frac{dF_d}{m_b} + \frac{dF_s}{dF_d}\frac{dF_s}{m_b}\right)\xi_1 \\ -\left(\frac{k_t}{m_w}\frac{dF_d}{m_w} + \frac{dF_s}{dF_d}\frac{dF_s+k_t}{m_w}\right)\xi_1 + \frac{k_t}{m_w}\xi_2 + \frac{dF_s}{dF_d}\xi_3 - \xi_4 \\ -\frac{k_t}{m_w}\xi_1 - \frac{dF_s}{dF_d}\xi_2 + \xi_3 - \frac{dF_d}{dF_s}\xi_4 \\ \frac{k_t}{m_w}\xi_1 + \frac{dF_s}{dF_d}\xi_2 - \xi_3 - \frac{m_w}{k_t}\frac{dF_s}{dF_d}\xi_4 \end{bmatrix}}{\frac{k_t}{m_w}\frac{dF_d}{m_b} + \frac{dF_s}{m_b}\frac{dF_s}{dF_d}}. \tag{35}$$

The observation matrix pair (A, C) has the same form as (32).

$$b(y) = \left[-\frac{dF_d}{m_e}y_1, -\left(\frac{dF_s}{m_e} + \frac{k_t}{m_w}\right)y_1, -\frac{k_t}{m_w}\frac{dF_d}{m_b}y_1, -\frac{k_t}{m_w}\frac{dF_s}{m_b}y_1\right]^T. \tag{36}$$

3) Under sensor placement configuration ③, the solution existing condition is a linear damping force. The solution is:

$$h = z_b - z_w, \quad y = z_b - z_w. \tag{37}$$

$$X(\xi) = \left[-\frac{dF_d}{m_b}\xi_1 + \frac{m_w}{k_t}\xi_4, \frac{dF_d}{m_w}\xi_1 - \xi_2 + \frac{m_w}{k_t}\xi_4, \xi_1, -\xi_1 + \frac{m_w}{k_t}\xi_3\right]^T \tag{38}$$

The observation matrix pair (A, C) has the same form as (32)

$$b(y) = \left[-\frac{dF_d}{m_e}y_1, -\frac{k_t}{m_w}y_1 - \frac{F_s(y_1)}{m_e}, -\frac{k_t}{m_w}\frac{dF_d}{m_b}y_1, -\frac{k_t}{m_w}\frac{F_s(y_1)}{m_b}\right]^T. \tag{39}$$

4) Under sensor placement configuration ④, the solution existing condition is a linear damping force. The solution is

$$h = h_1 = \dot{z}_b - \dot{z}_w, \quad y = y_1 = \dot{z}_b - \dot{z}_w. \tag{40}$$

$$x = X(\xi) = \left[\frac{m_w}{k_t}\xi_3, -\xi_1 + \frac{m_w}{k_t}\xi_3, -\frac{m_w}{k_t}\frac{m_b}{dF_s}\xi_4, \frac{m_w}{k_t}\xi_2 - \left(\frac{m_w}{k_t}\right)^2\frac{m_b}{m_e}\xi_4\right]^T. \tag{41}$$

The observation matrix pair (A, C) has the same form as (32).

$$b(y) = \left[-\frac{F_d(y_1)}{m_e}, -\left(\frac{dF_s}{m_e} + \frac{k_t}{m_w}\right)y_1, -\frac{k_t}{m_w}\frac{F_d(y_1)}{m_b}, -\frac{k_t}{m_w}\frac{dF_s}{m_b}y_1\right]^T. \tag{42}$$

5) Under sensor placement configuration ⑤, the solution existing condition is a linear damping and spring force. The solution

$$h = \left[-\frac{F_d(x_1-x_2)}{m_b} - \frac{F_s(x_3)}{m_b}, \dot{z}_b\right]^T, y = \left[\ddot{z}_b, \dot{z}_b\right]^T. \tag{43}$$

$$x = X(\xi) = \frac{\begin{bmatrix} \left(\frac{k_t}{m_w}\frac{dF_d}{m_b} + \frac{dF_s}{dF_d}\frac{dF_s}{m_b}\right)\xi_2 \\ -\frac{k_t}{m_w}\xi_1 + \frac{dF_s}{dF_d}\xi_3 - \xi_4 \\ -\frac{dF_s}{dF_d}\xi_1 - \left(\frac{k_t}{m_w}\frac{dF_d}{dF_s}\frac{dF_d}{m_b} + \frac{dF_s}{m_b}\right)\xi_2 + \xi_3 - \frac{dF_d}{dF_s}\xi_4 \\ \frac{dF_s}{dF_d}\xi_1 - \xi_3 - \frac{m_w}{k_t}\frac{dF_s}{dF_d}\xi_4 \end{bmatrix}}{\frac{k_t}{m_w}\frac{dF_d}{m_b} + \frac{dF_s}{dF_d}\frac{dF_s}{m_b}}. \tag{44}$$

$$A = \begin{bmatrix} 0, & 0, & 1, & 0 \\ 0, & 0, & 0, & 0 \\ 0, & 0, & 0, & 1 \\ 0, & 0, & 0, & 0 \end{bmatrix}, \quad C = \begin{bmatrix} 1, & 0, & 0, & 0 \\ 0, & 1, & 0, & 0 \end{bmatrix}. \tag{45}$$

$$b(y) = [-\frac{dF_d}{m_e}y_1 - \frac{dF_s}{m_b}y_2, y_1, -\frac{dF_s + k_t}{m_w}y_1, -\frac{dF_d}{m_b}\frac{k_t}{m_w}y_1 - \frac{dF_s}{m_b}\frac{k_t}{m_w}y_2]^T. \tag{46}$$

6) Under sensor placement configuration ⑥, there is no specific limit on the spring and damping force for the existence of the solution. The solution is

$$h = \left[\dot{z}_b - \dot{z}_w, z_b - z_w\right]^T, y = \left[\dot{z}_b - \dot{z}_w, z_b - z_w\right]^T. \tag{47}$$

$$x = X(\xi) = \left[\frac{m_w}{k_t}\xi_4, -\xi_1 + \frac{m_w}{k_t}\xi_4, \xi_2, \frac{m_w}{k_t}\xi_3\right]^T. \tag{48}$$

The observation matrix pair (A, C) has the same form as (45)

$$b(y) = [-\frac{F_s(y_2)}{m_e} - \frac{F_d(y_1)}{m_e}, y_1, -\frac{k_t}{m_w}y_1, -\frac{k_t}{m_w}\frac{F_s(y_2)}{m_b} - \frac{k_t}{m_w}\frac{F_d(y_1)}{m_b}]^T. \tag{49}$$

7) Under sensor placement configuration ⑦, the solution existing condition is a linear damping force. The solution is

$$h = \left[-\frac{F_d(x_1 - x_2)}{m_b} - \frac{F_s(x_3)}{m_b}, z_w - z_g\right]^T. \tag{50}$$

$$y = \left[\ddot{z}_b, z_b - z_w\right]^T. \tag{51}$$

The observation matrix pair (A, C) has the same form as (45)

$$b(y) = \begin{bmatrix} -\frac{dF_d}{m_e}y_1 + \frac{dF_s(y_2)}{dF_d}\frac{m_b y_1 + F_s(y_2)}{m_b} \\ -\frac{m_b y_1 + F_s(y_2)}{dF_d} \\ -\frac{k_t}{m_w}\frac{m_b y_1 + F_s(y_2)}{m_b} \\ -\frac{k_t}{m_w}\frac{dF_d}{m_b}y_1 \end{bmatrix}. \tag{52}$$

8) Under sensor placement configuration ⑧, the solution existing condition is a linear damping force. The solution is

$$h = \left[z_b - z_w, \dot{z}_b\right]^T, y = \left[z_b - z_w, \dot{z}_b\right]^T. \tag{53}$$

$$x = X(\xi) = \left[-\frac{dF_d}{m_b}\xi_1 + \xi_2, \frac{dF_d}{m_w}\xi_1 - \xi_3, \xi_1, -\xi_1 + \frac{m_w}{k_t}\xi_4\right]^T. \tag{54}$$

$$A = \begin{bmatrix} 0, & 0, & 1, & 0 \\ 0, & 0, & 0, & 0 \\ 0, & 0, & 0, & 1 \\ 0, & 0, & 0, & 0 \end{bmatrix}, \quad C = \begin{bmatrix} 1, & 0, & 0, & 0 \\ -\frac{dF_d}{m_b}, & 1, & 0, & 0 \end{bmatrix}. \tag{55}$$

$$b(y) = [-\frac{dF_d}{m_w}y_1 + y_2, -\frac{F_s(y_1)}{m_b}, -\frac{F_s(y_1)}{m_w} - \frac{k_t}{m_w}y_1, \frac{k_t}{m_w}y_2]^T. \tag{56}$$

9)Under sensor placement configuration ⑨, the solution existing condition is a linear damping and spring force. The solution is

$$h = \left[-\frac{F_d(x_1 - x_2)}{m_b} - \frac{F_s(x_3)}{m_b}, \dot{z}_b - \dot{z}_w\right]^T. \tag{57}$$

$$y = \left[\dot{z}_b, \dot{z}_b - \dot{z}_w\right]^T. \tag{58}$$

$$x = X(\xi) = [\xi_2 - \frac{dF_d}{m_b}\frac{m_w}{k_t}\xi_4, \frac{m_b}{dF_d}\xi_1 - \frac{dF_d}{m_b}\frac{m_w}{k_t}\xi_4, -\frac{dF_d}{dF_s}\xi_2, -\frac{dF_d}{m_b}\frac{m_w}{k_t}\xi_3]^T. \tag{59}$$

The observation matrix pair (A, C) has the same form as (55).

$$b(y) = [-\frac{dF_d}{m_e}y_1 - \frac{dF_s}{m_b}y_2, -\frac{dF_s}{dF_d}y_2, -\frac{k_t}{m_w}y_2, -\frac{k_t}{m_w}y_1]^T. \tag{60}$$

10) Under sensor placement configuration ⑩, the solution existing condition is a linear spring force. The solution is

$$h = \left[\dot{z}_b, \dot{z}_b - \dot{z}_w\right]^T, y = \left[\dot{z}_b, \dot{z}_b - \dot{z}_w\right]^T. \tag{61}$$

$$x = X(\xi) = [\xi_1, \xi_1 - \xi_2, -\frac{m_b}{dF_s}\xi_3, -\frac{m_b + m_w}{dF_s}\xi_3 + \frac{m_w}{k_t}\xi_4]^T. \tag{62}$$

The observation matrix pair (A, C) has the same form as (45).

$$b(y) = [-\frac{F_d(y_2)}{m_b}, -\frac{F_d(y_2)}{m_e}, -\frac{dF_s}{m_b}y_2, -\frac{dF_s}{m_e}y_2 + \frac{k_t}{m_w}y_1]^T. \tag{63}$$

The feedback linearization problem solution existing conditions under different sensor placement configurations are summarized in the table below.

As shown in Table 2, configuration ⑥ has the strongest universality; its observability and solvability are not affected by the form of the damping force and spring force. Therefore, sensor placement configuration ⑥ is chosen in our observer design process.

D. KALMAN FILTER OBSERVER DESIGN

Apply (28) to the suspension system state space, to obtain

$$b(y) = \dot{\xi} - A\xi = \begin{bmatrix} \dot{\xi}_1 - \xi_3 \\ \dot{\xi}_2 \\ \dot{\xi}_3 - \xi_4 \\ \dot{\xi}_4 \end{bmatrix} = \begin{bmatrix} -\frac{F_d(y_1)}{m_e} - \frac{F_s(y_2)}{m_e} \\ \dot{x}_3 \\ -\frac{k_t}{m_w}y_1 \\ -\frac{k_t}{m_w}\frac{F_s(y_2) + F_d(y_1)}{m_b} \end{bmatrix}. \tag{64}$$

TABLE 2. System observability and solvability under different sensor placement configurations.

Sensor configurations	Observability of the system	Solvability of the system under	
		Nonlinear spring force	Nonlinear damping force
①	√		
②	√		
③	√	√	
④	√		√
⑤	√		
⑥	√	√	√
⑦	√	√	
⑧	√	√	
⑨	√		
⑩	√		√

Considering noise, the transformed linear system state space is

$$\begin{cases} \dot{\xi} = A\xi + b(y) + Bw_\xi \\ y = C\xi + v_\xi \end{cases}. \tag{65}$$

where w_ξ is process noise and v_ξ is the measurement noise.

The measurement noise which is determined by the measurement system is not affected by the coordinate transfer, so now we have

$$v_\xi = v. \tag{66}$$

In order to get the noise coefficient B we can first of all assume $v_\xi = 0$, then we have

$$b(y) = b(C\xi), \tag{67}$$

$$\dot{\xi} = A\xi + b(\mathrm{C}y) + B_1 w_\xi. \tag{68}$$

Substitute the coordinate transfer into (68) and compare the coefficients with (4) to obtain

$$B_1 = \left[-\frac{k_t}{m_w}\ 0\ 0\ 0\right]^T. \tag{69}$$

Consider process noise,

$$y = C\xi + v_\xi. \tag{70}$$

$$\dot{\xi} = A\xi + b(C\xi) + B_1 z_g \approx A\xi + b(y) + B_1 z_g - \frac{\partial b}{\partial y}v_\xi. \tag{71}$$

where $\frac{\partial b}{\partial y} = \begin{bmatrix} -\frac{dF_d(y_1)}{m_e} & 1 & -\frac{k_t}{m_w} & -\frac{k_t}{m_w}\frac{dF_d(y_1)}{m_b} \\ -\frac{dF_s(y_2)}{m_e} & 0 & 0 & -\frac{k_t}{m_w}\frac{dF_s(y_2)}{m_b} \end{bmatrix}^T$.

define $w_\xi = \left[v_\xi, \dot{z}_g\right]^T$; we can obtain the noise matrix coefficient

$$B = \begin{bmatrix} -\frac{dF_d(y_1)}{m_e} & -\frac{dF_s(y_2)}{m_e} & -\frac{k_t}{m_w} \\ 1 & 0 & 0 \\ -\frac{k_t}{m_w} & 0 & 0 \\ -\frac{k_t}{m_w}\frac{dF_d(y_1)}{m_b} & -\frac{k_t}{m_w}\frac{dF_s(y_2)}{m_b} & 0 \end{bmatrix}. \tag{72}$$

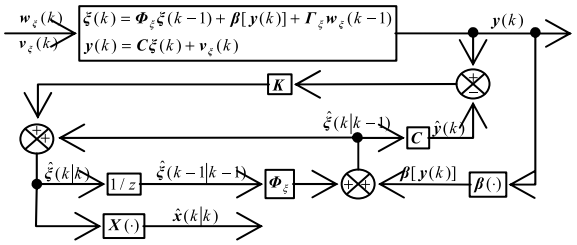

FIGURE 4. Flowchart of feedback linearization Kalman filter algorithm.

Now the original nonlinear system is linearized, and the linear Kalman filter can be applied to the linearized system.

Then, the linear Kalman algorithm can be applied to the linearized system, and state information ξ of the linearized system can be estimated. The state information of the original system can be obtained through an inverse coordinate transfer of ξ.

The discretized form of the linearized system under sample time t_s is

$$\begin{cases} \xi(k) = \Phi_\xi \xi(k-1) + \beta[y(k)] + \Gamma_\xi w_\xi(k-1), \\ y(k) = C\xi(k) + v_\xi(k). \end{cases} \tag{73}$$

where Φ_ξ, Γ_ξ and C are constant value matrixed; $\beta(\cdot)$ is the mapping of the output function.

E. ADAPTIVE PARAMETER CORRECTION FOR THE FILTER

The mismatch of the preset value of the covariance matrix of the process noise and the actual process noise may lead to a significant deviation of the observation results or even a divergence of the observing algorithm.

One advantage of the feedback linearization technique is that it is easy to apply mature linear observer design techniques to the linearized form of the system. In this section, we apply a widely used adaptive Kalman filter algorithm to the linearized form of the nonlinear system to improve the performance of the system under a disturbance.

For a given discretized linear system, who has the state space of:

$$\begin{cases} x(k) = \Phi(k-1)x(k-1) + \Theta(k-1)u(k-1) \\ +\Gamma(k-1)w(k-1), \\ y(k) = H(k)x(k) + v(k). \end{cases} \tag{74}$$

where $\Phi(k)$, $\Theta(k)$, $\Gamma(k)$ and $H(k)$ are system matrices;$Q(k)$ and $R(k)$ are the covariance matrices of the process noise $w(k)$ and the measurement noise $v(k)$ respectively. The above discretized linear system can also be the system who has been linearized by the feedback linearization process shown in our paper.

The flowcharts of a standard linear Kalman filter and adaptive Kalman filter are shown in Figure 5 and Figure 6.

We can see the difference between the standard Kalman filter and the adaptive Kalman filter is the process noise adaptive adjustment module.

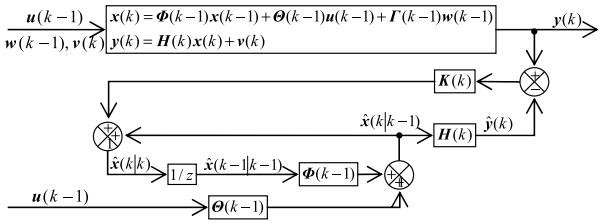

FIGURE 5. Flowchart of the standard Kalman filter algorithm.

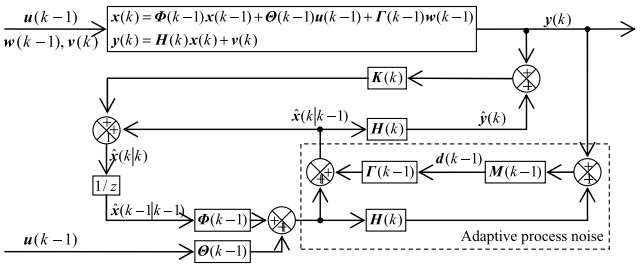

FIGURE 6. Flowchart of adaptive Kalman filter algorithm.

The specific algorithm for standard Kalman filter is

$$\hat{x}(k|k-1) = \Phi(k-1)\hat{x}(k-1|k-1) + \Theta(k-1)u(k-1). \tag{75}$$

$$P(k|k-1) = \Phi(k-1)P(k-1|k-1)\Phi^T(k-1) + \Gamma(k-1)Q(k-1)\Gamma^T(k-1). \tag{76}$$

$$K(k) = P(k|k-1)H^T(k)[H(k)P(k|k-1)H^T(k) + R(k)]^{-1}. \tag{77}$$

$$\hat{x}(k|k) = \hat{x}(k|k-1) + K(k)[y(k) - H(k)\hat{x}(k|k-1)]. \tag{78}$$

$$P(k|k) = [I - K(k)H(k)]P(k|k-1). \tag{79}$$

where, the hat operator Λ stands for an estimate of a variable. $(k|k-1)$ and $(k|k)$ denote the prior and posterior estimates of variables severally. P is the error covariance and K is the Kalman gain.

We can see there is a process noise adaptive module shown in Figure 6 where the gain matrix $M(k-1)$ is:

$$M(k-1) = [W + \Gamma^T(k-1)H^T(k) H(k)\Gamma(k-1)]^{-1}\Gamma^T(k-1)H^T(k). \tag{80}$$

where $d(k)$ is the model error and W is the weight coefficient matrix.

And the main difference between adaptive Kalman and standard Kalman is at the calculation of prior error covariance.

$$P(k|k-1) = \Phi(k-1)P(k-1|k-1)\Phi^T(k-1) + [N(k-1) + N^T(k-1)] + \Gamma(k-1) \times \{E[\langle d(k-1)\rangle] + Q(k-1)\}\Gamma^T(k-1). \tag{81}$$

$$E[\langle d(k-1)\rangle] = M(k-1)[\langle H(k)\Gamma(k-1)d(k-1)\rangle + R(k)]M^T(k-1). \tag{82}$$

$$N(k-1) = \Phi(k-1)P(k-1|k-1)\Phi^T (k-1)H^T(k)M^T(k-1)\Gamma^T(k-1). \tag{83}$$

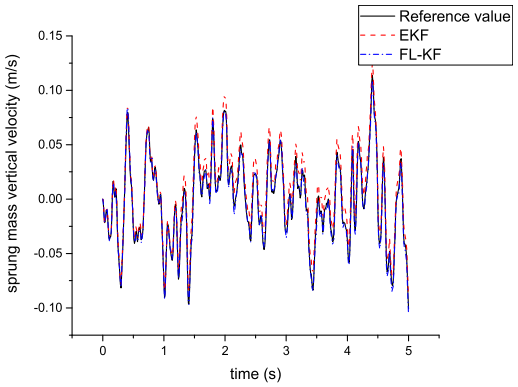

FIGURE 7. Sprung mass vertical speed simulation test estimation result grade-B random road profile.

where $\langle a \rangle \equiv aa^T$, $E[\langle d(k-1) \rangle]$ is the covariance matrix of $d(k-1)$; $N(k-1)$ is the cross-covariance matrix of $\Phi(k-1)[x(k-1) - \hat{x}(k-1|k-1)]$ and $\Gamma(k-1)d(k-1)$. The adaptive adjustment term $E[\langle d(k-1) \rangle]$ and $N(k-1)$ can compensate for the influence caused by the inaccuracy of the process noise covariance matrix. When the preset parameters of the observer are accurate, the adaptive Kalman filter should have the same outcome of standard Kalman.

IV. OBSERVER SIMULATION VERIFICATION

To verify the designed observer, simulation tests are performed in a MATLAB/Simulink environment under different road profiles. Estimation results output by the designed feedback linearization Kalman filter observer (FL-KF) and the extended Kalman filter (EKF), which have been widely applied in industrial, are compared.

A. OBSERVING RESULTS UNDER STANDARD ROAD PROFILE

For the estimation results listed below, a standard grade-B random road profile is adopted as the external road excitation, and the speed of the vehicle is maintained at 10 m/s.

To obtain a quantitative analysis of the estimation results, the accuracy index is defined.

$$accuracy = \left[1 - \frac{\sqrt{\sum_{k=1}^{N} \left(x(k) - \hat{x}(k)\right)^2}}{\sqrt{\sum_{k=1}^{N} (x(k))^2}}\right] \times 100\% \quad (84)$$

where x is the system state information, $\hat{x}$ is corresponding estimated value, and N is the number of discrete samples. A larger accuracy index value indicates the estimated system state is closer to the original system state, which indicates better accuracy; while the value of the accuracy index is no more than one.

The time-domain estimation results shown in Figures 7 to Figure 11 and the accuracy indexes listed in Table 3 indicate that the estimation results of all five system states output by our designed FL-KF observer algorithm are more precise than the estimation results output by the EKF algorithm under a grade-B road profile. However, the accuracy of the FL-KF

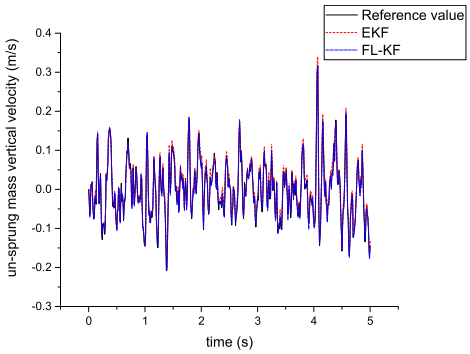

FIGURE 8. Un-sprung mass speed simulation test estimation result grade-B random road profile.

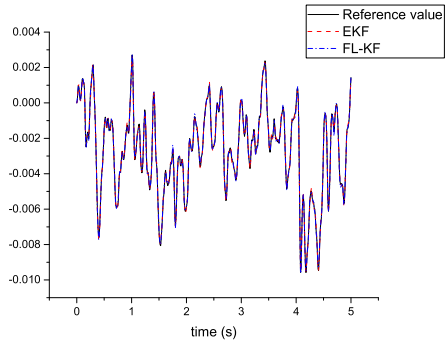

FIGURE 9. Suspension deflection simulation test estimation result grade-B random road profile.

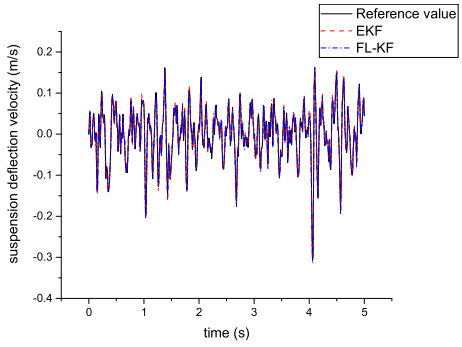

FIGURE 10. Suspension deflection speed simulation test estimation result grade-B random road profile.

and the EKF are different when estimating different system state information. Accuracy for both observers is relatively higher when estimating suspension deflection and suspension deflection speed. In addition, the difference between the accuracy of those two observers are smaller and even unnoticeable for the estimation results of suspension deflection and suspension deflection speed compared to the estimation results of other system states, which is because those two system states are also the measurement input of our designed observer whose value can be obtained by installed sensors.

To verify the designed observer under different road levels, simulation tests under ISO standard grade-A and grade-C level roads are also performed. Accuracy indexes under all three road levels are listed below.

Table 4 indicates that the designed observer remains accurate and is more accurate than the EKF under the three

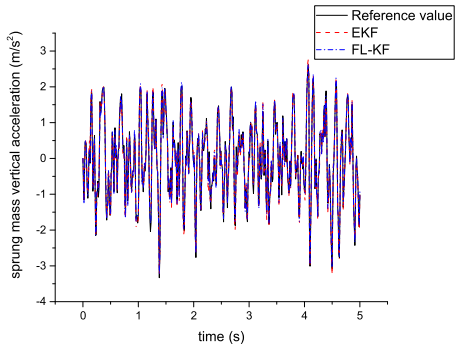

FIGURE 11. Sprung mass vertical acceleration simulation test estimation result grade-B random road profile.

TABLE 3. Accuracy indexes comparison under a grade-B road.

Estimated variables	Symbols	Accuracy index of EKF	Accuracy index of FL-KF
Vertical velocity of the sprung mass	V_ms	70.7	92.1
Vertical velocity of the un-sprung mass	V_mu	79.5	90.0
Suspension deflection velocity	V_sus	85.8	90.0
Vertical acceleration of the sprung mass	A_ms	85.2	89.3
Suspension deflection	D_sus	96.6	96.7

TABLE 4. Accuracy index comparison under different road levels.

Symbols of variables	Accuracy indexes of estimated variables under /%					
	A grade-A road		A grade-A road		A grade-A road	
	EKF	FL-KF	EKF	FL-KF	EKF	FL-KF
V_ms	77.4	94.2	70.7	92.1	62.4	90.2
V_mu	84.3	92.3	79.6	90.1	73.1	88.7
V_sus	91.4	93.1	85.7	90.2	84.5	88.1
A_ms	88.5	91.7	85.4	89.3	83.3	88.5
D_sus	96.9	97.1	96.5	96.9	92.6	93.2

different road levels. The accuracies of the FL-KF and the EKF under the grade-A road profile and grade-C road profile share the same trend as the accuracy when under the grade-B road profile; both observers have better performance when estimating suspension deflection and suspension deflection speed. The reason for this phenomenon was explained above. The difference between the estimation results of the FL-KF and the EKF becomes more obvious when the road excitation increases, which is because the error caused by the Taylor expansion and first-order approximation, which is used by the EKF as system linearization technique, increases when the system state is driven farther away from the equilibrium position by severe road excitation.

B. OBSERVING RESULTS UNDER A DISTURBANCE

To verify our designed adaptive estimator. Simulation experiment has been done under a grade-B road profile, the preset covariance value of the process noise is 0.01 times the actual value. The results of the simulation tests are listed below. FL-AKF stands for estimation results of feedback linearization Kalman filter with adaptive parameter correction.

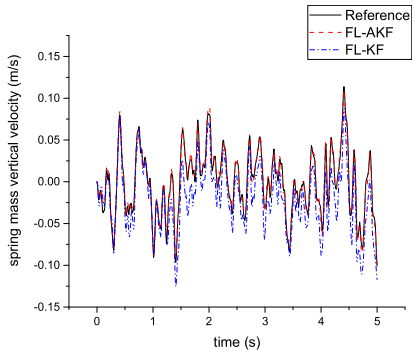

FIGURE 12. Sprung mass vertical speed simulation test estimation result under disturbance.

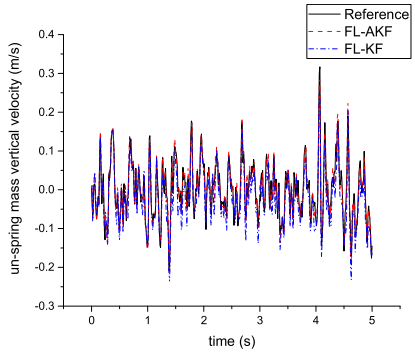

FIGURE 13. Un-sprung mass speed simulation test estimation result under disturbance.

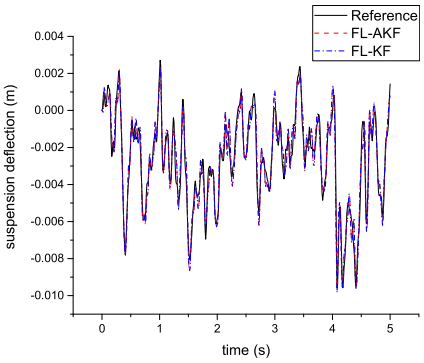

FIGURE 14. Suspension deflection simulation test estimation result under disturbance.

From above Figure 12 to Figure 16 and Table 5, we can figure out that the adaptive parameter correction module significantly improved the accuracy of the feedback linearization Kalman filter under the disturbance of the process noise. FL-AKF can effectively eliminate inaccuracy caused by the inaccurate process noise covariance.

V. MODE REFERENCE SLIDING MODE CONTROLLER DESIGN

The basic principle of the model reference control is to force a given system to behave as the desired system by introducing a proper controlling input. One advantage of model reference control is that the desired system, also known as the reference model, can be any model, even practically unfeasible model. In the case of a model reference sliding mode controller,

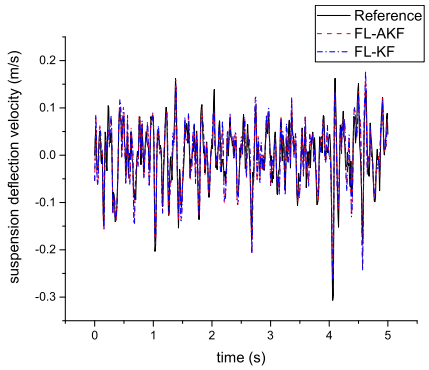

FIGURE 15. Suspension deflection speed simulation test estimation under disturbance.

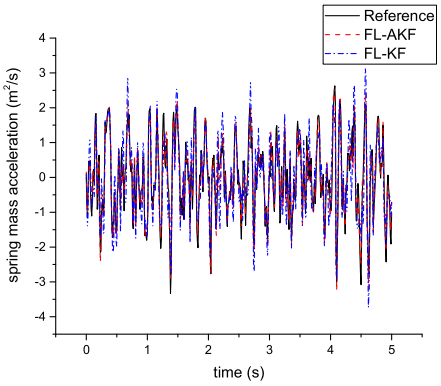

FIGURE 16. Sprung mass vertical acceleration simulation test estimation under disturbance.

TABLE 5. Accuracy indexes comparison under disturbance.

Parameters	Accuracy index of the FL-KF	Accuracy index of the FL-AKF
Vertical velocity of the sprung mass	70.8	89.2
Vertical velocity of un-sprung mass	79.8	86.4
Suspension deflection velocity	85.9	90.0
Vertical acceleration of the sprung mass	85.2	84.4
Suspension deflection	95.2	95.6

the difference between the reference response provided by the reference model and the response of the actual system is compensated by the sliding mode controller.

Proposed by Karnopp, skyhook control is a classic controller for semi-active suspension systems. In skyhook control theory, the spring mass is suspended by an imaginary damper between the spring mass and the sky. Therefore, the vertical acceleration of the spring mass can be minimized. However, setting a damper between the spring mass and the sky is obviously unpractical. In addition, skyhook control is often used as a reference mode in the suspension controller design process.

The control logic of skyhook control can be expressed as:

$$F_{\text{sky}} = \begin{cases} C_{\text{sky}}(\dot{z}_b - \dot{z}_w) & \dot{z}_b(\dot{z}_b - \dot{z}_w) > 0, \\ 0 & \dot{z}_b(\dot{z}_b - \dot{z}_w) < 0. \end{cases} \tag{85}$$

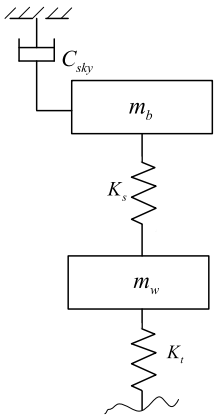

FIGURE 17. Sky-hook reference model.

The dynamic equation of the spring mass under skyhook control is

$$m_b\ddot{z}_b = F_s(z_b - z_w) + F_d(\dot{z}_b - \dot{z}_w) - C_{\text{sky}} \cdot \dot{z}_b \tag{86}$$

where C_{sky} is the skyhook damping coefficient.

The aim of the proposed sliding mode controller is to make the spring mass track the motion of the reference model. According to the motion equations of the spring mass of the actual system and the reference model.

The tracking error of the controller is defined as:

$$e = \dot{z}_{bd} - \dot{z}_b \tag{87}$$

where $\dot{z}_{bd}$ is the spring-mass vertical velocity of the reference model.

The sliding mode surface is defined as

$$S = \lambda \int edt + e \tag{88}$$

Differentiate the above equation to obtain

$$\dot{S} = \lambda e + \dot{e} \tag{89}$$

Define $\gamma = \lambda e + \ddot{z}_{sd} - f_s; f_s = F_s/m_s; G = 1/m_s$ and consider system perturbation to obtain

$$\begin{aligned} \dot{S} &= \lambda e + (\ddot{z}_{sd} - \ddot{z}_s) \\ &= \lambda e + \ddot{z}_{sd} - f_s - \Delta f_s - Gu - \Delta Gu \\ &= \gamma - \Delta f_s - Gu - \Delta Gu \end{aligned} \tag{90}$$

where Δf_s is the system perturbation; ΔG is the vehicle mass perturbation.

Then, the equivalent control law is

$$u_{\text{eq}} = G^{-1}\gamma \tag{91}$$

With no loss of generality, the sliding mode control law has the form of

$$u = u_{\text{eq}} + G^{-1}u_s \tag{92}$$

where u_s is the switch control representing the feedback control constraining the perturbation of the system.

To verify the stability of the sliding mode controller, define the Lyapunov function

$$V = \frac{1}{2}S^2 \tag{93}$$

The necessary and sufficient condition for stability of the sliding mode controller is that the Lyapunov function subject to the following function

$$\frac{dV}{dt} = S\dot{S} < 0 \tag{94}$$

Substitute (92) into (94) to obtain

$$\frac{dV}{dt} = S\left[-\Delta f_s - u_s - \Delta GG^{-1}\gamma - \Delta GG^{-1}u_s\right] \tag{95}$$

Define the system uncertainty boundary as $\Delta f_s \leq \rho_f$, $\Delta GG^{-1} \leq \rho$. Design the switch control law as

$$u_s = \frac{\varepsilon}{1-\rho} sign(S) \tag{96}$$

Substitute (92) into (95) to obtain

$$\frac{dV}{dt} \leq \|S\|\left[\rho_f - \frac{\varepsilon}{1-\rho}\frac{S}{\|S\|} + \rho\|\gamma\| + \rho\frac{\varepsilon}{1-\rho}\frac{S}{\|S\|}\right] \tag{97}$$

$$\frac{dV}{dt} \leq \|S\|\left[\rho_f - \varepsilon\frac{S}{\|S\|} + \rho\|\gamma\|\right] \leq \|S\|\left[\rho_f + \rho\|\gamma\| - \varepsilon\right] \tag{98}$$

where, $\|\cdot\|$ is the Euclidean norm.

When $\varepsilon = \rho_f + \rho\|\gamma\|$, we have

$$\frac{dV}{dt} \leq 0 \tag{99}$$

The stability of the designed sliding mode controller is then proven.

To reduce chattering, the saturation function is introduced to the switch control law

$$u_s = \frac{\varepsilon}{1-\rho} Sat(S) \tag{100}$$

where $Sat(S) = \begin{cases} 1 & \frac{S}{\delta} > 1 \\ \frac{S}{\delta} & \left|\frac{S}{\delta}\right| < 1 \\ -1 & \frac{S}{\delta} < -1 \end{cases}$ δ is a small positive constant.

The designed sliding mode controller works with the observer in a cooperative way. Which is shown in the figure below.

As shown in the figure above, the suspension deflection and suspension deflection rate signals are measured by the sensors implemented on the vehicle as the input for the FL-AKF observer. The vertical speed of the vehicle body as the output of the observer is then sent to the controller. The suspension deflection rate is also sent to the controller directly. With those two variables, the sliding mode controller is able to calculate the corresponding control current for the semi-active suspension.

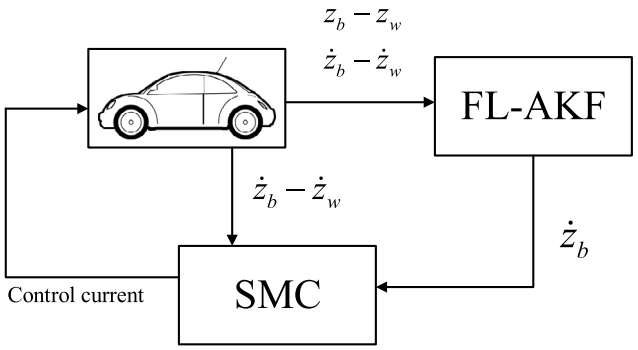

FIGURE 18. Flowchart of observer based sliding mode controller.

VI. TEST RIG EXPERIMENT

A. EXPERIMENTAL SETUP

The performance of the designed observer was investigated through simulation tests in the previous section and the designed observer seems to be effective. Effectiveness of the designed feedback linearization Kalman filter based sliding mode controller is verified in this section through a real test bench environment. The ability of the observer to provide accurate enough state information for the semi-active suspension system controller is then verified through the rig test.

The bench test setup is shown in Figure 19. The test rig is designed to analyse the vertical motion behaviour of a quarter car system. Mass blocks are used to represent the spring mass of the car. Spiral springs are used to represent the spring force of the suspension spring and the spring force of the tyre. The road profile is simulated by an excitation head, which is powered by a hydraulic oil source. The excitation part, whose type is sy70, is based on a test stand from Dongling Tech. Two LVDT sensors that have been installed on the test stand can take the displacement signal of the spring mass and relative displacement signal of the spring mass and unsprung mass. Observe and control algorithms are implemented in a dSPACE AutoBox controller in the form of a rapid control prototype (RCP).

As shown in Figure 20, the displacement signals sent from the LVDT sensors are inputted to the observing and controlling algorithms through a data acquisition card integrated with the AutoBox controller. Experiment data are also collected in the same way and stored in the host PC. The vertical displacement signal of the spring mass, which is estimated by the feedback linearization Kalman filter algorithm, is sent to the model reference sliding mode controller together with the suspension deflection speed signal measured and differentiated from the LVDT sensor. The controller sends a PWM signal, whose duty cycle corresponds to the desired damping force, to the driving module, which consists of a DC power supply and a MOSFET driver. A certain control current is then outputted by the driving module to the adjustable damper. The electro valve of the damper reacts to the current correspondingly, and thus changes the damping force of the damper.

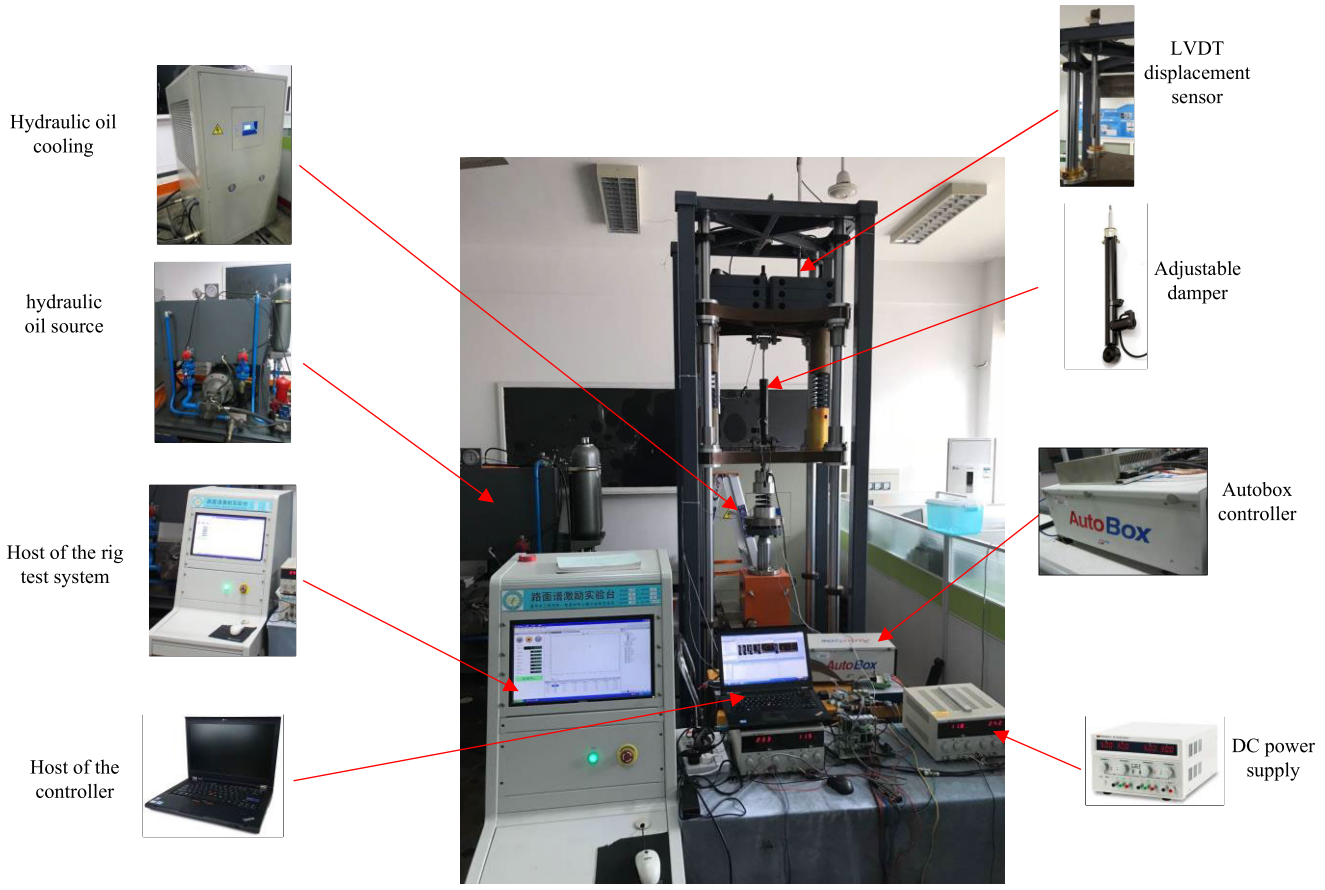

FIGURE 19. Semi-active suspension rig test system.

From the flowchart of our observer-based model reference sliding mode controller, we find that in the working process of our designed controller, it is important to calculate a corresponding control current according to the desired damping force and suspension speed. Thus, a three-dimensional lookup table is made according to the damping force character we obtained in section II.

From Figure 21 we determine that when the direction of the suspension speed and desired damping force are not considered, for a certain desired damping force, the corresponding control current decreases when the suspension speed increases.

B. ESTIMATION RESULTS ANALYSIS

To verify the designed observing and control algorithm, rig test is performed under typical road profiles which are ISO standard grade-C random road and sine road excitation (with an amplitude of 25 mm and frequency of 1 Hz). The speed of the vehicle is maintained at 10 m/s for both road profiles.

From the flowchart shown in Figure 19, we determine that the estimated state information needed by the controlling algorithm in our case is mainly the vertical speed of the spring mass. Other state information is either irrelevant to the controlling algorithm or can be measured directly by sensors. Therefore, to verify the ability of the designed observer to provide accurate enough state information for the controller in the test rig environment, only the estimation result of the vertical speed of the spring mass is listed here.

From Figure 22 and Figure 23, it can be seen that though estimation seems to be slightly underestimated the designed observer can follow the vertical speed of the spring mass well. Compared to the estimation results in the simulation test, the estimation seems to be delayed, that time delay is caused by the computational process of the estimation algorithm. Quantitative analysis of the estimation results is also performed. For estimation results under the grade-C random road profile, the accuracy of the estimation result defined in (84) is 85.84%, slightly less than the accuracy under the simulation environment under the same road profile and vehicle speed. The maximum error of the estimation results under the sine road profile occurred at 4.39 s in the time domain, the error is 0.01385 m/s with the reference value 0.06349 m/s and estimation value 0.04964 m/s. Although the error seems to be unneglectable at the peak value of the sine wave, the estimation follows the reference value quite well at other parts.

C. CONTROLLING RESULTS ANALYSIS

The performance of the designed controller is verified in terms of sprung/unsprung mass acceleration and suspension deflection in both the time and frequency domain.

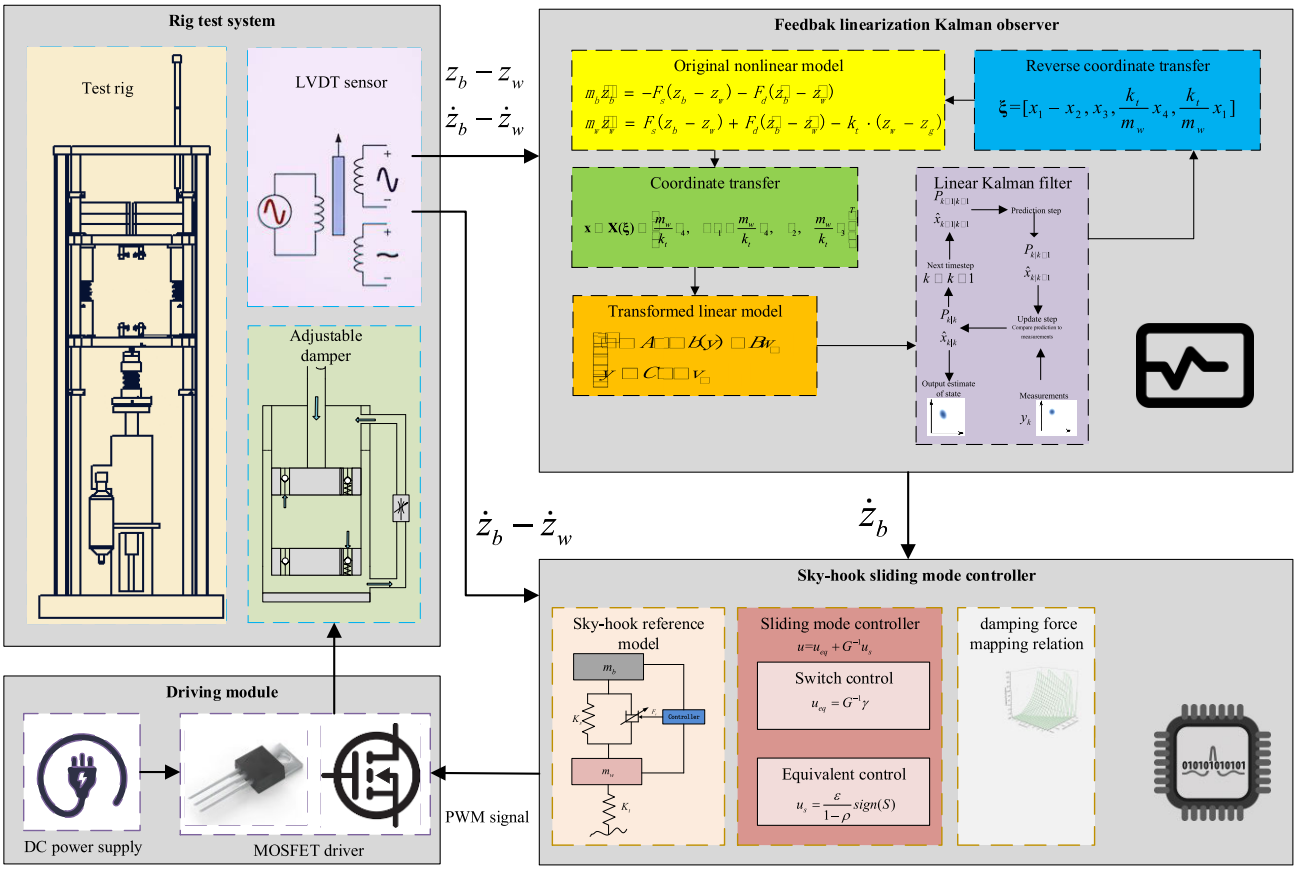

FIGURE 20. Flowchart of the semi-active suspension rig test system.

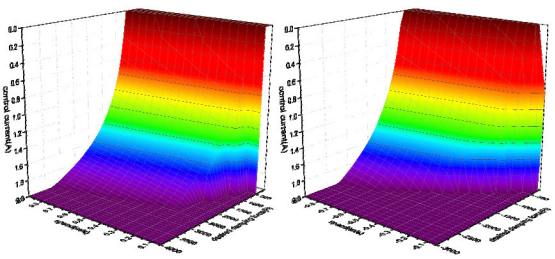

FIGURE 21. Three dimension table to calculate corresponding control current according to the desired damping force and suspension speed of compress stroke (left) and recover stroke (right).

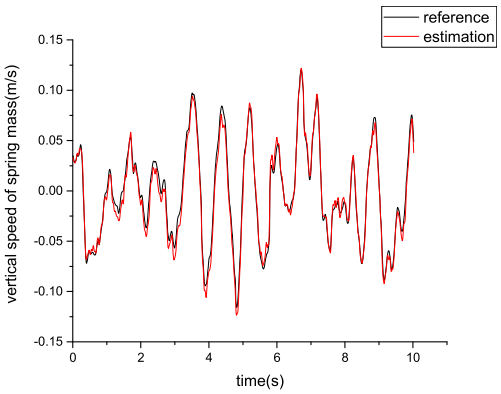

FIGURE 22. Sprung mass vertical speed rig test estimation result grade-C road profile.

1) RANDOM ROAD PROFILE

The results below are under the ISO standard grade-C road profile; vehicle speed was maintained at 10 m/s.

Where in Figure 24 to Figure 26, passive indicates that the adjustable damper is set to medium damping force mode and no control algorithm is applied. Semi-active indicates that the FL-KF based sliding mode controller is applied to the suspension system. PSD in the frequency domain presents power spectral density. From Figure 24, we can determine the overall acceleration value of spring mass decreases when the designed controller is applied, which indicates that the ride comfort of the vehicle improved. The improvement is more significant in the low-frequency range of the frequency domain. In terms of suspension deflection, the application of the designed controller also lowers the overall suspension deflection value; again, the improvement is more significant in the low-frequency range. However, Figure 26 shows the peak-peak value of the unsprung mass dynamic load increases when the controller is applied, especially in the frequency range of 8-12 Hz. The same trend can be found in the RMS (root mean square) character of the above results. With the help of our designed observer-based controller, the RMS

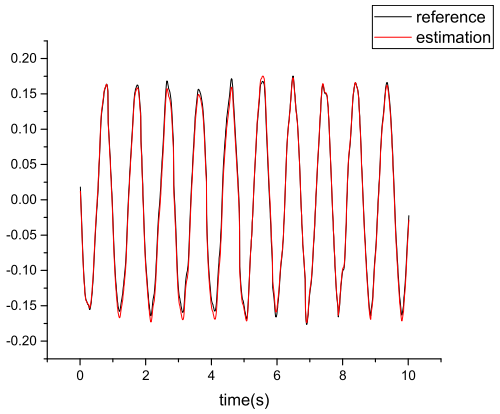

FIGURE 23. Sprung mass vertical speed rig test estimation result sine road profile.

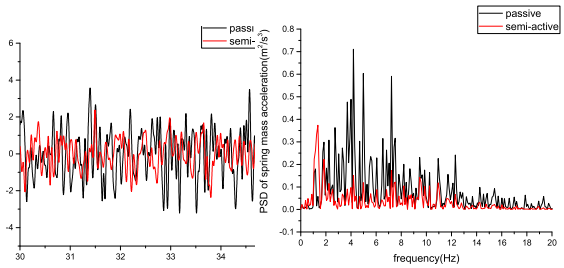

FIGURE 24. Time-domain (left) and frequency-domain (right) of sprung mass acceleration in the rig test under a grade-C profile.

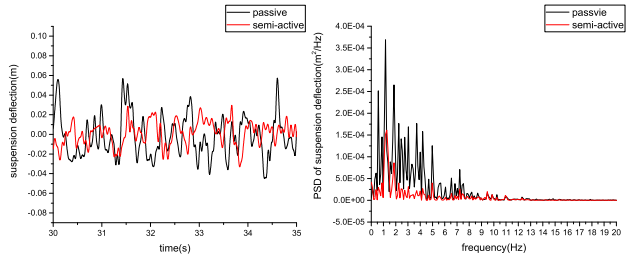

FIGURE 25. Time-domain (left) and frequency-domain (right) of suspension deflection in the rig test under a grade-C profile.

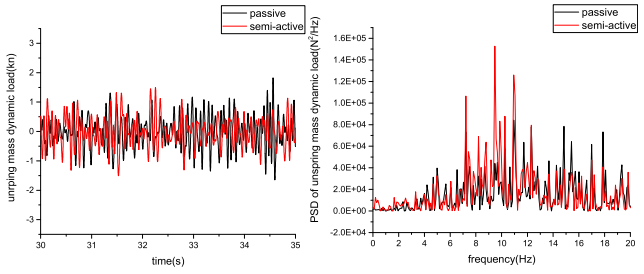

FIGURE 26. Time-domain (left) and frequency-domain (right) of unsprung mass dynamic load in the rig test under a grade-C profile.

of spring-mass acceleration drops from 1.2074 to 0.9408, and the RMS of suspension deflection drops from 0.0238 to 0.0157. However, the RMS of the unsprung mass dynamic load increases from 0.5411 to 0.5794. The character of the experimental result of the designed controller is identical to the reference skyhook model; ride comfort of the vehicle

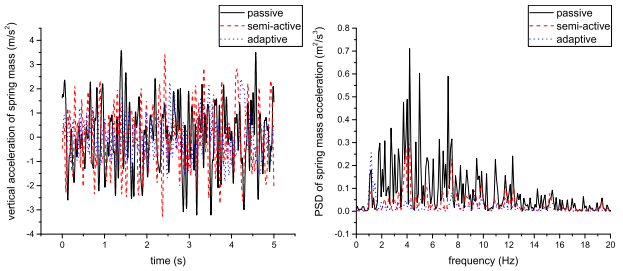

FIGURE 27. Time-domain (left) and frequency-domain (right) of spring mass acceleration in the rig test under a grade-C profile and a disturbance.

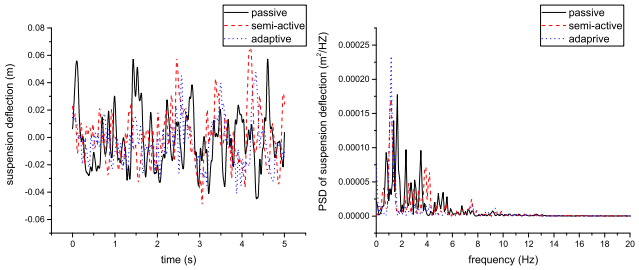

FIGURE 28. Time-domain (left) and frequency-domain (right) of suspension deflection in the rig test under a grade-C profile and a disturbance.

can be significantly improved with the cost of increasing the dynamic load of the unsprung mass.

2) RANDOM ROAD PROFILE UNDER A DISTURBANCE

To verify the proposed controller under the condition of parameter variations. The sliding mode controller combined with the FL-KF and the FL-AKF respectively are tested under an ISO standard grade-C road profile, the vehicle speed is maintained at 10 m/s. The preset process noise covariance value is set to 0.01 times the actual value. The inaccurate process noise covariance value is regarded as the disturbance of the system parameter in our test.

Where in Figure 27 to Figure 29, passive indicates that the adjustable damper is set to medium damping force mode and no control algorithm is applied. Semi-active indicates that the FL-KF based sliding mode controller has been applied to the suspension system and adaptive indicates that the FL-AKF based sliding mode controller has been applied to the suspension system. From the above figures, it is obvious that under the condition of parameter variation, the FL-AKF based controller shows better performance compared to the FL-KF based controller. That is because the FL-AKF estimator has been proved to have better accuracy under parameter variation when estimating system state information. And the inaccurate state information outputted by FL-KF will cause deterioration in the performance of the sliding mode controller. Our designed FL-AKF based controller significantly improves the ride comfort of the vehicle even under the condition of parameter variation.

3) SINE ROAD PROFILE

Under sine road excitation with an amplitude of 25 Hz and a frequency of 1 Hz.

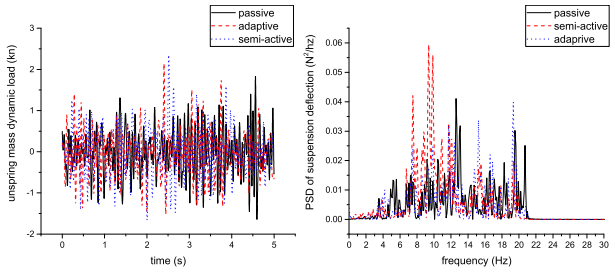

FIGURE 29. Time-domain (left) and frequency-domain (right) of unsprung mass dynamic load in the rig test under a grade-C profile and a disturbance.

TABLE 6. RMS value comparison.

RMS value of \ Controller	Passive	Semi-active	Adaptive
Spring mass acceleration	1.2074	1.12	0.99
Suspension deflection	0.0238	0.02084	0.0186
Unsprung mass dynamic load	0.5411	0.5528	0.5634

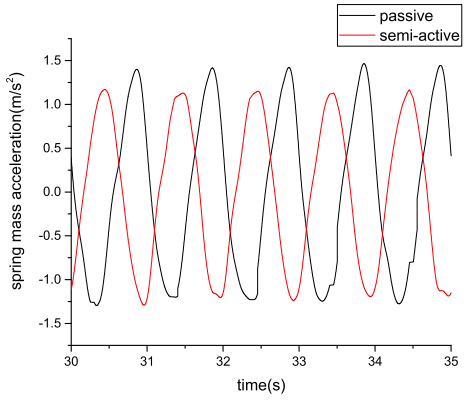

FIGURE 30. Acceleration of spring mass under sine road excitation.

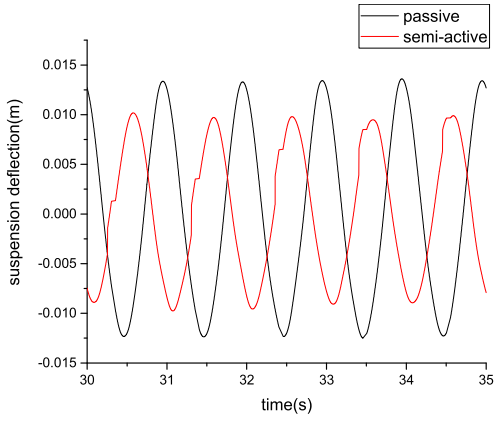

FIGURE 31. Suspension deflection under sine road excitation.

From Figure 30, we can determine that with the help of our observer based sliding mode controller, the maximum peak-peak value of spring mass acceleration drops from 2.841 to 2.696, and the maximum peak-peak value of the suspension deflection decreases from 0.02632 to 0.02013. The maximum peak-peak value of the unsprung mass dynamic load increases from 120.3 to 134.8, which means

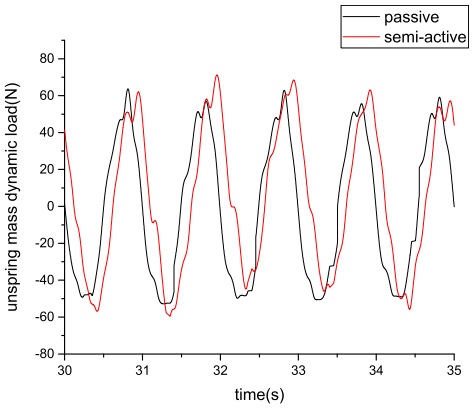

FIGURE 32. Unsprung mass dynamic load under sine road excitation.

the controller successfully improves the vehicle ride comfort under sine road excitation and significantly reduces the possibility of bump stopper impact with the cost of a slight increase in the unsprung mass dynamic load. The performance of the designed controller under sine road excitation is identical to its performance under random road profiles.

VII. CONCLUSION AND FUTURE WORK

In this paper, an observer based on feedback linearization was designed. A quarter car nonlinear suspension system model was built based on the damping force characteristic of the adjustable damper acquired from the experiment. Possible sensor placement configurations for the quarter vehicle observer design problem were listed, and system observability and solvability under those sensor placement configurations were analyzed based on a geometry differential. A certain coordinate transfer for the nonlinear system was found to transform the original nonlinear system into a linear system. A Kalman filter algorithm was then applied to the transformed linear system. The state information of the original system was then obtained through inverse coordinate transfer. The designed observer was verified under different typical road profiles in a simulation test and proved to be effective and superior to a recent technique. A model reference sliding mode controller based on the observer was proposed. A suspension rig test system was implemented; both the observer and observer-based controller was verified in a rig test environment. To improve the performance of the designed observer and observer based controller under disturbances. An adaptive parameter correction technique is introduced to the observer. It is proven that the adaptive parameter correction technique can improve the accuracy of the feedback linearization Kalman filter observer under a given disturbance in a simulation test, and thus, improve the performance of observer based sliding mode controller under a given disturbance in a rig test. The designed observer-based semi-active suspension controller effectively improves ride comfort with commonly used and low-cost sensors and shows significant robustness to parameter variations.

APPENDIX

$$m_e = \frac{m_b \times m_w}{m_b + m_w}, dF_d = \frac{d}{d(x_1 - x_2)} F_d, dF_s = \frac{d}{dx_3} F_s$$

$$d^{i+1}F_d = \frac{d}{d(x_1 - x_2)} d^i F_d, d^{i+1}F_s = \frac{d}{dx_3} d^i F_s, \quad i = 1, 2, 3$$

$$A_1 = \frac{d^2F_d}{m_e}\left(\frac{F_d}{m_e} + \frac{F_s}{m_e} - \frac{k_t}{m_w}x_4\right) + \left(\frac{dF_d}{m_e}\right)^2 - \frac{dF_s}{m_e}$$

$$A_2 = \frac{dF_d}{m_e}\frac{dF_s}{m_e} - \frac{d^2F_s}{m_e}(x_1 - x_2)$$

$$\begin{aligned} A_3 = & -\frac{dF_d}{m_e}A_1 + A_2 - \frac{d^3F_d}{m_e}\left(\frac{F_d}{m_e} + \frac{F_s}{m_e} - \frac{k_t}{m_w}x_4\right)^2 \\ & -3\frac{d^2F_d}{m_e}\frac{dF_d}{m_e}\left(\frac{F_d}{m_e} + \frac{F_s}{m_e} - \frac{k_t}{m_w}x_4\right) \\ & +\left(\frac{d^2F_d}{m_e}\frac{dF_s}{m_e} - \frac{d^2F_s}{m_e}\right)\cdot(x_1 - x_2) - \frac{k_t}{m_w}\frac{d^2F_d}{m_e}x_2 \end{aligned}$$

$$\begin{aligned} A_4 = & -\frac{dF_s}{m_e}A_1 - \left(\frac{F_d}{m_e} + \frac{F_s}{m_e} - \frac{k_t}{m_w}x_4\right) \\ & \times\left(\frac{d^2F_d}{m_e}\frac{dF_s}{m_e} - \frac{d^2F_s}{m_e}\right) \\ & +\left[\frac{dF_d}{m_e}\frac{d^2F_s}{m_e} - \frac{d^3F_s}{m_e}(x_1 - x_2)\right]\cdot(x_1 - x_2) + \frac{k_t}{m_w}\frac{dF_s}{m_w} \end{aligned}$$

$$A_5 = \frac{k_t}{m_w}\left[A_1 + \frac{d^2F_d}{m_e}\left(\frac{F_d}{m_e} + \frac{F_s}{m_e} - \frac{k_t}{m_w}x_4\right) - \left(\frac{k_t}{m_w}\right)\right]$$

REFERENCES

[1] P. T. Venhovens, "The development and implementation of adaptive semi-active suspension control," *Vehicle Syst. Dyn.*, vol. 23, no. 1, pp. 211–235, 1994.

[2] A. Hac and I. Youn, "Optimal semi-active suspension with preview based on a quarter car model," *J. Vibrat. Acoust.*, vol. 114, no. 1, pp. 84–92, Jan. 1992.

[3] D. Hrovat, D. L. Margolis, and M. Hubbard, "An approach toward the optimal semi-active suspension," *J. Dyn. Syst., Meas., Control*, vol. 110, no. 3, pp. 288–296, Sep. 1988.

[4] H. C. Sohn, K. S. Hong, and J. K. Hedrick, "Semi-active control of the Macpherson suspension system: Hardware-in-the-loop simulations," in *Proc. IEEE Int. Conf. Control Appl.*, Sep. 2000, pp. 982–987.

[5] M. Ahmadian, "A hybrid semiactive control for secondary suspension applications," in *Proc. 6th ASME Symp. Adv. Automot. Technol.*, 1997, pp. 743–750.

[6] D. Karnopp, M. J. Crosby, and R. A. Harwood, "Vibration control using semi-active force generators," *J. Eng. Ind.*, vol. 96, no. 2, pp. 619–626, May 1974.

[7] G. D. Buckner, K. T. Schuetze, and J. H. Beno, "Active vehicle suspension control using intelligent feedback linearization," in *Proc. IEEE Amer. Control Conf.*, Jun. 2000, pp. 4014–4018.

[8] B. Lin, X. Su, and X. Li, "Fuzzy sliding mode control for active suspension system with proportional differential sliding mode observer," *Asian J. Control*, vol. 21, no. 1, pp. 264–276, Jan. 2019, doi: 10.1002/asjc.1882.

[9] X. Ma, P. K. Wong, and J. Zhao, "Practical multi-objective control for automotive semi-active suspension system with nonlinear hydraulic adjustable damper," *Mech. Syst. Signal Process.*, vol. 117, pp. 667–688, Feb. 2019, doi: 10.1016/j.ymssp.2018.08.022.

[10] S. D. Nguyen and T.-I. Seo, "Establishing ANFIS and the use for predicting sliding control of active railway suspension systems subjected to uncertainties and disturbances," *Int. J. Mach. Learn. Cybern.*, vol. 9, no. 5, pp. 853–865, May 2018.

[11] S. D. Nguyen, H.-V. Ho, T.-T. Nguyen, N. T. Truong, and T.-I. Seo, "Novel fuzzy sliding controller for MRD suspensions subjected to uncertainty and disturbance," *Eng. Appl. Artif. Intell.*, vol. 61, pp. 65–76, May 2017.

[12] S. D. Nguyen and Q. H. Nguyen, "Design of active suspension controller for train cars based on sliding mode control, uncertainty observer and neuro-fuzzy system," *J. Vibrat. Control*, vol. 23, no. 8, pp. 1334–1353, May 2017.

[13] Y. Qin, F. Zhao, Z. Wang, L. Gu, and M. Dong, "Comprehensive analysis for influence of controllable damper time delay on semi-active suspension control strategies," *J. Vibrat. Acoust.*, vol. 139, no. 3, p. 31006, Jun. 2017.

[14] B.-K. Song, J.-H. An, and S.-B. Choi, "A new fuzzy sliding mode controller with a disturbance estimator for robust vibration control of a semi-active vehicle suspension system," *Appl. Sci.*, vol. 7, no. 10, p. 1053, Oct. 2017, doi: 10.3390/app7101053.

[15] D. X. Phu, S. Choi, Y. Lee, and M. Han, "Vibration control of a vehicle's seat suspension featuring a magnetorheological damper based on a new adaptive fuzzy sliding-mode controller," *Proc. Inst. Mech. Eng. D, J. Automobile Eng.*, vol. 230, no. 4, pp. 437–458, 2016.

[16] H. Ren, S. Chen, Y. Zhao, G. Liu, and L. Yang, "State observer-based sliding mode control for semi-active hydro-pneumatic suspension," *Vehicle Syst. Dyn.*, vol. 54, no. 2, pp. 168–190, Feb. 2016, doi: 10.1080/00423114.2015.1122818.

[17] J.-L. Yao, W.-K. Shi, J.-Q. Zheng, and H.-P. Zhou, "Development of a sliding mode controller for semi-active vehicle suspensions," *J. Vibrat. Control*, vol. 19, no. 8, pp. 1152–1160, Jun. 2013, doi: 10.1177/1077546312441045.

[18] J. Yao and J. Zheng, "Semi-active suspension system design for quarter-car model using model reference sliding mode control," in *Proc. IEEE Int. Conf. Veh. Electron. Saf.*, Dec. 2006, pp. 398–402.

[19] A. Aldair and W. Wang, "A neurofuzzy controller for full vehicle active suspension systems," *J. Vibrat. Control*, vol. 18, no. 12, pp. 1837–1854, Oct. 2012.

[20] H.-Y. Chen and S.-J. Huang, "Functional approximation-based adaptive sliding control with fuzzy compensation for an active suspension system," *Proc. Inst. Mech. Eng. D, J. Automobile Eng.*, vol. 219, no. 11, pp. 1271–1280, Nov. 2005.

[21] H. Li, J. Yu, C. Hilton, and H. Liu, "Adaptive sliding-mode control for nonlinear active suspension vehicle systems using T–S fuzzy approach," *IEEE Trans. Ind. Electron.*, vol. 60, no. 8, pp. 3328–3338, Aug. 2013.

[22] F. Zhao, M. Dong, Y. Qin, L. Gu, and J. Guan, "Adaptive neural-sliding mode control of active suspension system for camera stabilization," *Shock Vibrat.*, vol. 2015, pp. 1–8, 2015.

[23] O. Yakut and H. Alli, "Neural based sliding-mode control with moving sliding surface for the seismic isolation of structures," *J. Vibrat. Control*, vol. 17, no. 14, pp. 2103–2116, Dec. 2011.

[24] C.-H. Chen, C.-J. Lin, and C.-T. Lin, "Nonlinear system control using adaptive neural fuzzy networks based on a modified differential evolution," *IEEE Trans. Syst., Man, Cybern. C, Appl. Rev.*, vol. 39, no. 4, pp. 459–473, Jul. 2009.

[25] S. D. Nguyen, S.-B. Choi, and Q. H. Nguyen, "A new fuzzy-disturbance observer-enhanced sliding controller for vibration control of a train-car suspension with magneto-rheological dampers," *Mech. Syst. Signal Process.*, vol. 105, pp. 447–466, May 2018, doi: 10.1016/j.ymssp.2017.12.019.

[26] L. Zhang, B. Li, H. Du, and B. Zhang, "Takagi–Sugeno fuzzy-based Kalman filter observer for vehicle side-slip angle estimation and lateral stability control," in *Proc. 3rd Int. Symp. Auton. Syst.*, May 2019, pp. 352–357.

[27] I. RubioScola, M. Patrone, D. Feroldi, and G. Besancon, "Observer-based controller for an electric vehicle with hybrid energy storage," in *Proc. Argentine Conf. Autom. Control (AADECA)*, 2018, pp. 1–6, doi: 10.23919/AADECA.2018.8577241.

[28] D. Viegas, P. Batista, P. Oliveira, and C. Silvestre, "Discrete-time distributed Kalman filter design for formations of autonomous vehicles," *Control Eng. Pract.*, vol. 75, pp. 55–68, Jun. 2018, doi: 10.1016/j.conengprac.2018.03.014.

[29] M. Z. Ernani, M. Bozorg, and S. Ebrahimi, "Identification of an autonomous underwater vehicle dynamic using extended Kalman filter with ARMA noise model," *Int. J. Robot.*, vol. 4, no. 1, pp. 22–28, 2015.

[30] G. Reina and A. Messina, "Vehicle dynamics estimation via augmented extended Kalman filtering," *Measurement*, vol. 133, pp. 383–395, Feb. 2019, doi: 10.1016/j.measurement.2018.10.030.

[31] W. Liu, H. He, and F. Sun, "Vehicle state estimation based on minimum model error criterion combining with extended Kalman filter," *J. Franklin Inst.*, vol. 353, no. 4, pp. 834–856, Mar. 2016, doi: 10.1016/j.jfranklin.2016.01.005.

[32] S. Yim, J. Seok, and J. Lee, "State estimation of the nonlinear suspension system based on nonlinear Kalman filter," in *Proc. IEEE Int. Conf. Control, Automat. Syst.*, Oct. 2012, pp. 720–725.
[33] B. L. Boada, M. J. L. Boada, and V. Diaz, "Vehicle sideslip angle measurement based on sensor data fusion using an integrated ANFIS and an unscented Kalman filter algorithm," *Mech. Syst. Signal Process.*, vols. 72–73, pp. 832–845, May 2016, doi: 10.1016/j.ymssp.2015.11.003.
[34] S. Olma, A. Kohlstedt, P. Traphöner, K.-P. Jäker, and A. Trächtler, "Observer-based nonlinear control strategies for Hardware-in-the-Loop simulations of multiaxial suspension test rigs," *Mechatronics*, vol. 50, pp. 212–224, Apr. 2018, doi: 10.1016/j.mechatronics.2017.10.007.
[35] A. E. Vela, D. H. Alcántara, R. M. Menendez, O. Sename, and L. Dugard, "H_∞ observer for damper force in a semi-active suspension," *IFAC-PapersOnLine*, vol. 51, no. 11, pp. 764–769, 2018, doi: 10.1016/j.ifacol.2018.08.411.
[36] A. Giua, M. Melas, C. Seatzu, and G. Usai, "Design of a predictive semi-active suspension system," *Vehicle Syst. Dyn.*, vol. 41, no. 4, pp. 277–300, Apr. 2004, doi: 10.1080/00423110412331315169.
[37] Y. Ma and Y. Cai, "A fuzzy model predictive control based upon adaptive neural network disturbance observer for a constrained hypersonic vehicle," *IEEE Access*, vol. 6, pp. 5927–5938, 2018.
[38] Z. Peng and J. Wang, "Output-feedback path-following control of autonomous underwater vehicles based on an extended state observer and projection neural networks," *IEEE Trans. Syst., Man, Cybern., Syst.*, vol. 48, no. 4, pp. 535–544, Apr. 2018.
[39] X. Chen, W. Shen, M. Dai, Z. Cao, J. Jin, and A. Kapoor, "Robust adaptive sliding-mode observer using RBF neural network for lithium-ion battery state of charge estimation in electric vehicles," *IEEE Trans. Veh. Technol.*, vol. 65, no. 4, pp. 1936–1947, Apr. 2016.
[40] B. Jiang, P. Shi, C. C. Lim, and D. Xu, "Adaptive neural observer-based backstepping fault tolerant control for near space vehicle under control effector damage," *IET Control Theory Appl.*, vol. 8, no. 9, pp. 658–666, Jun. 2014.
[41] M. Hou and A. C. Pugh, "Observer with linear error dynamics for nonlinear multi-output systems," *Syst. Control Lett.*, vol. 37, no. 1, pp. 1–9, 1999, doi: 10.1016/S0167-6911(98)00105-4.

ZHENG LIU received the M.S. degree from the University of Science and Technology, Beijing, in 2014. He is currently pursuing the Ph.D. degree with the School of Mechanical Engineering, Beijing Institute of Technology.

His research interests include vehicle dynamic and control, semi-active/active suspension systems, and relevant technologies of intelligent vehicles.

HONGBIN REN (Member, IEEE) received the Ph.D. degree in mechanical engineering from the Beijing Institute of Technology.

He was a Visiting Scholar with the University of Michigan-Dearborn, Dearborn, MI, USA, from 2012 to 2014. His current research interests include vehicle dynamics, state observer theory, motion planning, and optimization and optimal control.

SIZHONG CHEN received the M.S. degree from the College of Automotive Engineering, Jilin University, Beijing, China, in 1987. He is currently a Professor with the School of Mechanical engineering, Automotive Research Institute, Beijing Institute of Technology. His current research interests include suspension dynamics and steering, vehicle design, and control technology.

He serves as the Secretary-General for the SUV Technology Committee of the Society of Automotive Engineering of China.

YONG CHEN received the M.E. degree from the School of Mechanical Engineering, Beijing Institute of Technology, Beijing, China, in 2018, where he is currently pursuing the Ph.D. degree.

His research interests include electric vehicles, vehicle dynamic, and control and autonomous vehicles and relevant technologies of intelligent vehicles.

JIANBO FENG received the B.S. degree from the School of Mechanical Engineering and Automatic Control, Zhengzhou University, China, in 2012. He is currently pursuing the Ph.D. degree in mechanical and vehicular engineering.

His research interests include real-time 4WD control, chassis control, and integrated control.